Post-synthesis control of Berry phase driven magnetotransport in SrRuO₃ films

E. Skoropata [1,*] A. R. Mazza,[1] A. Herklotz,[1,2] J. M. Ok,[1] G. Eres,[1] M. Brahlek,[1] T. R. Charlton [3]
H. N. Lee,[1] and T. Z. Ward [1,†]

[1]*Materials Science and Technology Division, Oak Ridge National Laboratory, Oak Ridge, Tennessee 37830, USA*
[2]*Institute of Physics, Martin-Luther-University Halle-Wittenberg, Halle 06120, Germany*
[3]*Neutron Science Division, Oak Ridge National Laboratory, Oak Ridge, Tennessee 37830, USA*

Controlling electronic band structure is an important step toward harnessing quantum materials for practical uses. This is exemplified in the spin-polarized bands near the Fermi level of a ferromagnet where small variation to the Berry curvature can be used to control the intrinsic anomalous Hall effect (AHE). Since these pathways are highly sensitive to crystal structure, iterative post-synthesis manipulation of the underlying lattice can act as a fundamental probe and provide new opportunities for functionalization. In this work, depth-dependent magnetic inhomogeneity in a 4*d* itinerant ferromagnet SrRuO₃ film is controlled by applying low energy He ion irradiation. Combined magnetometry, polarized neutron reflectometry, and magnetotransport experiments demonstrate that the Berry phase and associated AHE can be continuously and iteratively modified post-synthesis. The findings of this work should be widely applicable to other quantum materials where crystal distortions and symmetry are tightly bound to band structure and resulting Berry phase effects.

I. INTRODUCTION

Manipulating magnetotransport properties that originate from topologically nontrivial characteristics of functional quantum materials can provide a foundation for future technology requiring fast energy efficient sensors and devices. For example, the intrinsic anomalous Hall effect (AHE) of conducting magnetic materials can be understood using the framework of band structure topology as it relates to modifying functionally relevant Berry phase curvature effects [1,2]. A consequence of the band-structure relationship is that the AHE is intimately connected to symmetry, spin-orbit coupling, and disorder. Large AHEs are also expected to originate from nontrivial nodal points in Weyl and three-dimenional (3D) Dirac semimetals [3,4]. More recently, in systems hosting chiral spin textures like skyrmions, an additional topological Hall effect (THE) with dramatic field-dependent anomalies results from an emergent electromagnetic field and Berry phase in real space originating from the interaction of charge carriers with the magnetic spin topology [5,6]. Disentangling the unconventional magnetotransport signatures from real- and momentum-space Berry phases potentially existing simultaneously in complex materials systems [7–17]

remains a considerable challenge that hinders the precise control of electronic functionalities. Most importantly, by discovering new approaches to continuously alter the structure and symmetry of complex materials systems we can open new pathways to understand the origin of novel functional properties.

A model system that exemplifies the complexity of understanding unconventional magnetotransport is SrRuO₃. Here, Berry phase physics manifests in magnetotransport of this 4*d* itinerant ferromagnet as an unconventional temperature-dependent AHE attributed to topologically nontrivial t_{2g} band crossings near the Fermi level [7,18,19]. Difficulties in understanding and controlling the AHE responses are the result of the band structure being extremely sensitive to dimensional confinement, structural symmetry, and disorder [9,11–17,20–23]. Experimental approaches aimed at exploiting these sensitivities have relied on substrate- or interface-induced strain; however, these methods have proved incapable of providing the minute structural distortion and symmetry modifications that can be expected to be required for functionalization [24].

In this work, we demonstrate the continuous control of the intrinsic AHE in bulk-like films of 20 nm thickness by modifying lattice symmetry and unit-cell volume with low-energy helium ion irradiation to apply uniaxial lattice expansion along the film's out-of-plane direction [25–28]. We also provide an example of a fully experimental measure of the inhomogeneous ferromagnetism and intrinsic AHE with a depth-dependent magnetic profile measured using polarized neutron reflectometry to model the "hump-like anomaly" mimicking the topological Hall effect of SrRuO₃ that is fully consistent with the bulk-senstive magnetometry and magnetotransport behaviors. Our method to continuously tune magnetotransport resulting from the Berry phase mechanism

*Present address: Swiss Light Source, Paul Scherrer Institut, 5232 Villigen PSI, Switzerland.
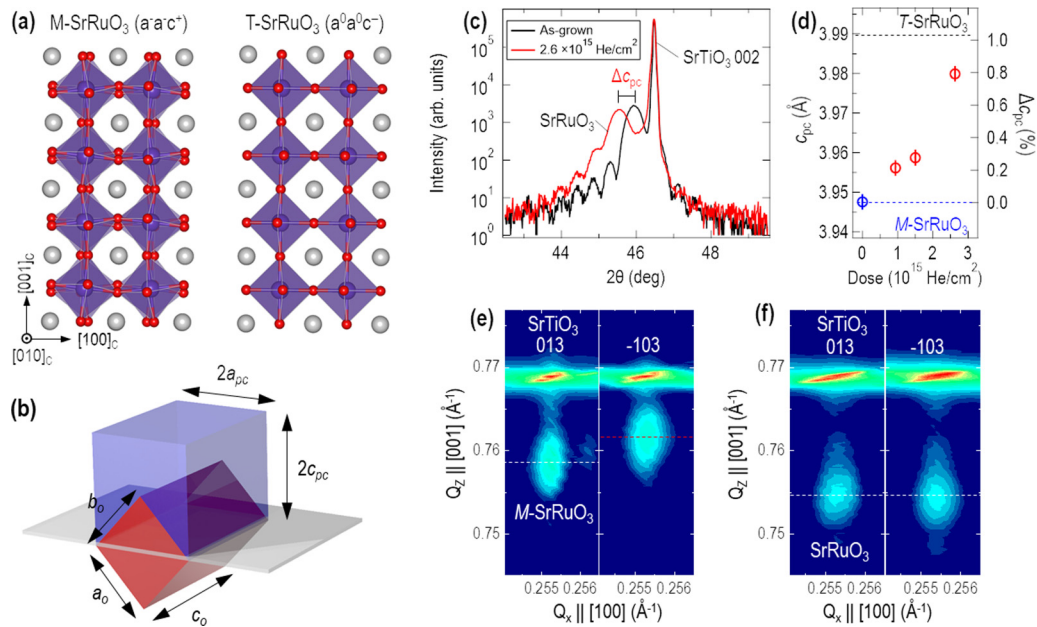†wardtz@ornl.gov

FIG. 1. (a) Illustration of the octahedral rotations of SrRuO$_3$ in the orthorhombic (*M*-SRO) and tetragonal (*T*-SRO) phases. (b) Epitaxial relationship between the *M*-SRO and pseudocubic (pc) indices. (c) θ–2θ scans of the SrRuO$_3$ thin films grown on SrTiO$_3$ (001) substrates with different helium dosages. (d) The out-of-plane lattice parameter changes as a function of the helium dose labeled according to the pseudocubic unit cell as c_{pc}. (e) Reciprocal space map around the $(103)_{pc}$ reflection of the as-grown sample is consistent with the typical orthorhombic phase, whereas (f) a nearly full transition to the undistorted tetragonal phase is indicated with the largest lattice expansion.

of SrRuO$_3$ opens the possibility to control topological properties arising from the lattice strain that reaches far beyond the epitaxial interface. Our work points to an alternative synthetic approach to control the underlying symmetries that are closely linked to novel quantum phenomena.

II. EXPERIMENTAL METHODS

SrRuO$_3$ films of 20 nm thickness are grown epitaxially on SrTiO$_3$ (001) substrates using pulsed laser deposition followed by iterative low-energy helium ion irradiation to modify out-of-plane lattice expansion and subsequent octahedral rotations [28]. To design a desired strain profile through the film thicknesses Stopping and Range of Ion Motion (SRIM) models are used to guide a selection of sacrificial gold cap layer thickness and ion acceleration voltages [28]. The cap layers are removed prior to magnetic and transport characterizations.

All samples were synthesized by pulsed laser epitaxy with a substrate temperature, oxygen partial pressure, and laser fluence of 700 °C, 100 mTorr, and 1.0 J/cm^2, respectively on atomically flat TiO$_2$-terminated (001) SrTiO$_3$ substrates with a KrF eximer laser ($\lambda = 248$ nm). The crystal structure, phase purity, and orientation of these films were confirmed by x-ray reflectivity and diffraction measurements using a Panalytical X'pert four-circle x-ray diffractometer. Samples were helium implanted using a SPECS IQE 11/35 ion source. The optimal conditions for controlling ion implantation cross sections in films of 20 to 30 nm can be achieved by varying a sacrificial gold cap layer of thicknesses ranging from 10 to 25 nm in concert with varying implantation energy between 4 and 5 keV.

The electronic transport measurements were performed with a 9 T Quantum Design PPMS (physical properties mea-

surement system). The electrical contacts were made with indium solder in a van der Pauw configuration, and the field-dependent data were antisymmetrized. The magnetization was determined with a 7 T Quantum Design MPMS3 (magnetic properties measurement system), after subtracting a linear background to correct for the diamagnetic response of the SrTiO$_3$ substrate [29].

Polarized neutron reflectivity was measured using the Magnetism Reflectometer (BL4A) located at the Spallation Neutron Source at Oak Ridge National Laboratory. An applied magnetic field of 4.7 T was provided by a warm-bore cryomagnet with the field direction parallel to the projection of the scattering plane onto the sample's surface. The sample was held in helium exchange gas at 2 K by a recondensing helium cryostat capable of providing a stable sample temperature between 1.8 and 800 K.

III. RESULTS AND DISCUSSION

Bulk and as-grown thin film SrRuO$_3$ adopts the *Pbnm* space group that is described by the Glazer notation $a^-a^-c^+$. With helium irradiation, a transformation to the tetragonal phase is accompanied by the removal of the rotations about the two in-plane axes to $a^0a^0c^-$ and an expansion of the lattice in the out-of-plane direction [28], as illustrated in Fig. 1. X-ray diffraction and reciprocal space maps (RSMs) of SrRuO$_3$ films demonstrate that even under the largest helium dose the film's quality and expansion along the out-of-plane direction can be controlled while maintaining epitaxy to the substrate. Consistent with previous studies, the RSMs about the (103) reflection indicate that the octahedral rotations present in the epitaxially strained orthorhombic phase of the as-grown film along the in-plane directions are gradually reduced as uniaxial
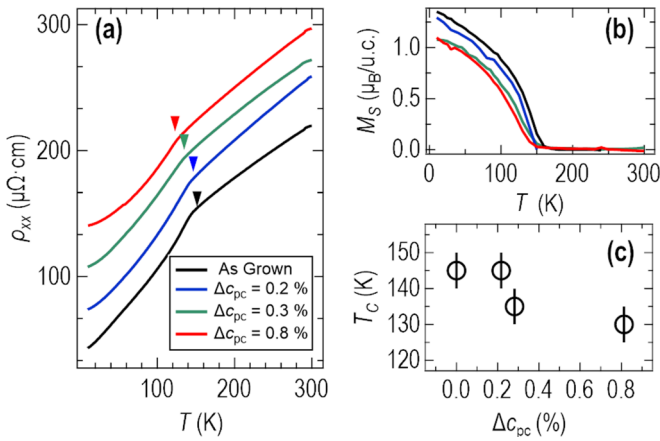
FIG. 2. (a) Resistivity ρ_{xx} and (b) saturation magnetization M_S, are shown as a function of temperature, in addition to (c) the ferromagnetic Curie temperature T_C determined from $\rho_{xx}(T)$.

out-of-plane expansion is applied [28,30,31]. The structural characterizations are used to quantify four different films with increasing lattice expansion. These states follow a relatively smooth transition from the as-grown orthorhombic state toward the most expanded out-of-plane lattice state which shows no orthorhombic distortions [28]. For simplicity, these states are described through the change in measured c_{pc}-axis lattice length (Δc_{pc}) from the as-grown state (Fig. 1).

The as-grown SrRuO$_3$ shows metallic behavior where the resistivity ρ_{xx} decreases with decreasing temperature. The

prominent change in slope of $\rho_{xx}(T)$ in Fig. 2(a) is due to a suppression of spin scattering on cooling to the ferromagnetic state [32] that was used to determine $T_C = 145$ K for the as-grown SrRuO$_3$ film. The saturation magnetization, M_S, at 10 K of 1.5 μ_B/unit cell, and $M_S(T)$ were consistent with the T_C indicated by $\rho_{xx}(T)$, and with the physical properties of other high quality epitaxial SrRuO$_3$ films [33,34]. An increase in ρ_{xx} and decrease in T_C and M_S are observed with progressively larger lattice expansions. The observed change in ρ_{xx} and small reduction in T_C is in agreement with the transformation from the orthorhombic to the tetragonal phase as unit cell volume is increased [35].

To map how the structural transformation impacts the magnetotransport properties, the Hall resistivity ρ_{xy} is measured as a function of out-of-plane applied magnetic field $H_\perp$ from 10 to 150 K for different lattice expansions and is shown in Fig. 3. In a conventional ferromagnet, the Hall resistivity is described by the empirical relation $\rho_{xy} = \rho_{OHE} + \rho_{AHE} = R_0 H_\perp + R_S M_\perp$, where the ordinary Hall coefficient (R_0) depends on the density of the charge carriers and the anomalous Hall resistivity follows the out-of-plane magnetization ($M_\perp$) through the coefficient (R_S) which depends on the longitudinal resistivity (ρ_{xx}). At the lowest temperatures, as-grown SrRuO$_3$ exhibits n-type carriers, as characterized by a negative linear ordinary Hall effect $\rho_{OHE} = R_0 H$, where $R_0 = 1/ne$ provides the carrier concentration $n = 1.8 \times 10^{22}$ cm^{-3}. The field dependence is characterized by a square-shaped $\rho_{AHE}(H)$ with the coercive field ($H_{C,AHE}$) required to reverse the sign of $\rho_{AHE}(H)$ at a fixed temperature. The magnitude of ρ_{AHE} is defined as the magnitude of $\rho_{xy}(H)$ well above the field-
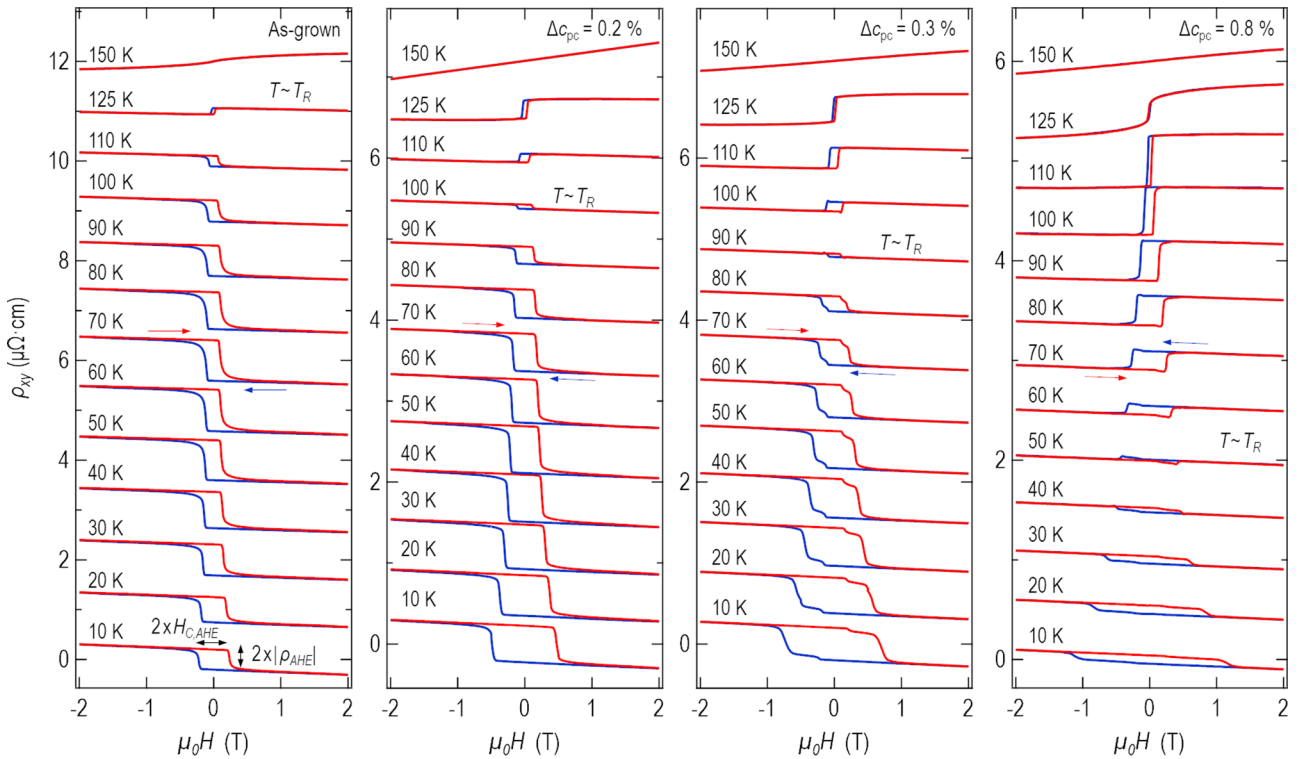

FIG. 3. Hall effect measurements of as-grown and helium irradiated SrRuO$_3$ films. Definitions for the anomalous Hall resistivity ρ_{AHE} and coercive field $H_{C,AHE}$ are indicated at curves for the as-grown film measured at 10 K. Note the scale differences labeled on the vertical axis, and curves at different temperatures are shown with a constant offset for clarity.
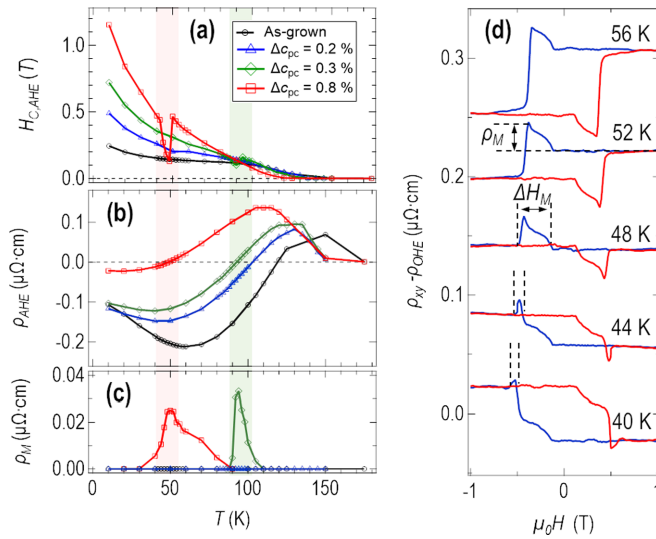
FIG. 4. The (a) zero crossing of the AHE with applied magnetic field, $H_{C,AHE}$, (b) ρ_{AHE}, and (c) peak amplitude of the hump-like feature ρ_M are shown for as-grown and helium irradiated films. (d) Detailed temperature scans of the largest lattice expanded film for $T \sim T_R$ showing the clear hump-like feature.
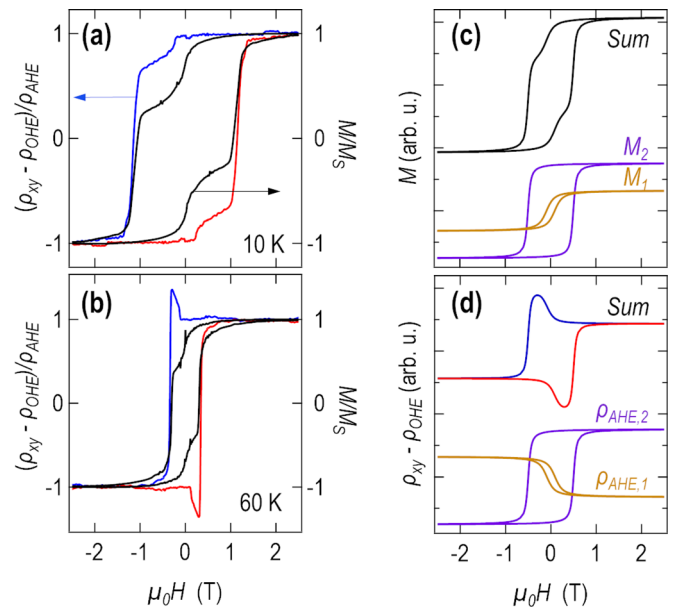

FIG. 5. A comparison of the normalized magnetization and anomalous Hall resistivity at (a) 10 K and (b) 60 K for helium irradiated SrRuO$_3$ with the largest lattice expansion. Illustration of multicomponent field-dependent reversal of the (c) magnetization and (d) Hall effect resistivity for two arbitrary superimposed components with opposite sign anomalous Hall coefficient and different magnetic coercivities.

dependent hysteresis, after subtracting the linear contribution from ρ_{OHE}. The observation that the anomalous Hall coefficient R_S has a negative value at low temperatures and changes sign at a reversal temperature $T_R \sim 130$ K is in agreement with previous reports of bulk and thin film SrRuO$_3$ that show an unconventional $\rho_{AHE}(T)$ due to k-space Berry phase effects [18].

It is evident that the magnetotransport properties summarized in Fig. 4 are all strongly influenced by structural modifications induced by helium irradiation. At 10 K, the as-grown SrRuO$_3$ shows a moderate $H_{C,AHE}$ typical of the approximate out-of-plane easy axis of the orthorhombic phase. A gradual but substantial increase in $H_{C,AHE}$ coincides with lattice expansion. This $H_{C,AHE}$ enhancement is consistent with a reorientation of the magnetic easy axis, which can be expected as lattice symmetry is shifted from an in-plane to out-of-plane tetragonality [36]. More intriguing, is the gradual tuning of the temperature dependence of $\rho_{AHE}(T)$ and T_R that signifies a change in the Berry phase mechanism induced in a macroscopic and controlled manner as the lattice is expanded. Since the electronic transport occurs within the RuO$_6$ network, changes in the unit cell volume or octahedral tilts and rotations are expected to modify the electronic properties due to the reduction of orbital overlap. Examining broadly the evolution of the Hall effect with uniaxial lattice expansion, there is a gradual tuning from the nearly all negative ρ_{AHE} behavior of the orthorhombic SrRuO$_3$ towards the tetragonal phase that displays a positive ρ_{AHE} at all temperatures [37–40]. This is consistent with a scenario in which an increase in the unit cell volume modifies the Ru-O hybridization to tune states near the Fermi level.

At higher levels of lattice expansion, $\rho_{xy}(H)$ also develops a complex shape including a prominent hump-like peak with $|\rho_{xy}(H)| < |\rho_{AHE}|$ around $T \sim T_R$, as shown in Figs. 4(c) and 4(d). This additional Hall resistivity is defined as ρ_M and

is quantified from the maximum deviation from ρ_{AHE}. To understand this unconventional field-dependent response, it is essential to compare the $M(H)$ and $\rho_{xy}(H)$ measured at the same temperatures to directly distinguish ferromagnetism from a potential noncollinear or chiral response. Although such a comparison is often overlooked in SrRuO$_3$ ultrathin films and heterostructures displaying the unconventional magnetotransport properties, a lack of consideration of both the magnetization and magonetotransport response can lead to statements on mechanisms that are inconclusive. Figures 5(a) and 5(b) show clear feature overlaps between these measurements within regions of similar applied magnetic fields. Furthermore, the $H_{C,AHE}$ of ρ_{xy} displays an apparent nonmonotonic temperature dependence in the vicinity of T_R for films with a hump-like feature. This behavior indicates that multiple decoupled spin populations are present within the film and that each spin population possesses distinct field reversal behaviors. The occurrence of a hump-like anomaly has been observed recently in ultrathin SrRuO$_3$ films and heterostructures, where inhomogeneities such as interfacial octahedral rotations are proposed to induce coexisting magnetic states within a SrRuO$_3$ film [20,37,40]. The *positive* hump-like anomaly in helium irradiated SrRuO$_3$ is quantitatively different from ultrathin SrRuO$_3$ and heterostructures, which display a *negative* hump (see Supplemental Material (SM) Fig. 1 [41]). This suggests that the effects of helium-induced lattice expansion alter the intrinsic properties of SrRuO$_3$ differently than natural epitaxial relaxation. Nevertheless, an interpretation based on inhomogeneous ferromagnetism, represented in the most simple case by two components with opposite AHE [Fig. 5(c)–5(d)], can produce
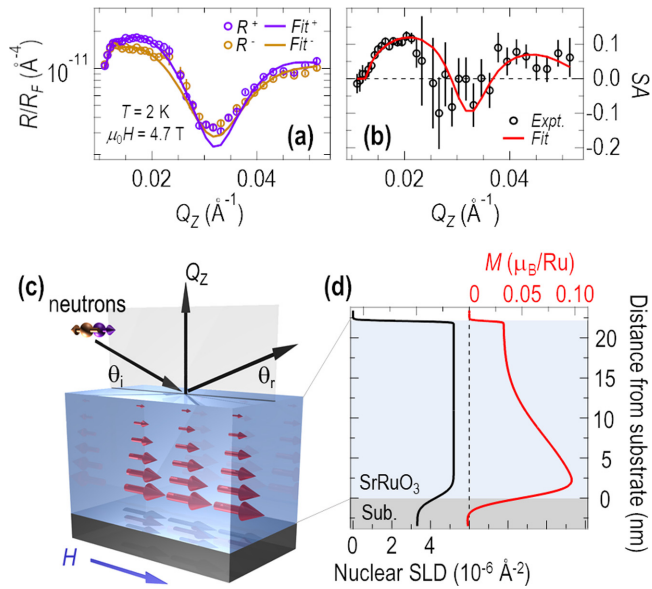
FIG. 6. Polarized neutron reflectometry (PNR) of helium irradiated $SrRuO_3$. The experimental and fitted normalized (a) neutron reflectivity (R/R_F) and (b) spin asymmetry (SA). (c) Illustration of the PNR experiment, and inhomogeneous magnetization profile of helium irradiated $SrRuO_3$ film. (d) The best fit of the depth-dependent nuclear density and magnetization profiles. Further detail of the fitting method used to obtain the result in (d) can be found in SM Sec. 3 [41].

FIG. 7. Anomalous Hall effect sign reversal modeled using the depth-dependent magnetic profile obtained from neutron experiments. (a) ρ_{xy} of the surface and interface components which define the limits of the profile distribution of the model (at 60 K), and (b) shown for all temperatures where the black line indicates the film average identical to Figs. 4(a) and 4(b). (c) Comparison of the experimental Hall effect measurement for the $SrRuO_3$ film with the largest c_{pc}-axis expansion, and the model from the PNR-derived inhomogeneity profile, and distribution in ρ_{xy} and H_C from (b).

the qualitative temperature-dependent change in $\rho_{xy}(T)$ of helium irradiated $SrRuO_3$.

While a model of the "hump-like anomaly" of $SrRuO_3$ based on inhomogeneous ferromagnetism appears compelling, a complete understanding of the physical properties requires an understanding of the origin of the magnetic homogeneity. To investigate the magnetization profile to determine the film uniformity directly, polarized neutron reflectometry (PNR) measurements were performed on a helium irradiated film. In an effort to observe possible magnetic inhomogeneity, PNR measurements were conducted in a magnetic field of 4.7 T at 2 K, well above fields showing magnetic hysteresis in Hall effect and magnetometry measurements. Fitting of the neutron and x-ray reflectivity data was done using Parratt formalism [42] using the REFL1D software package [43]. Fits to the PNR data (normalized to R_F = asymptotic value of the Fresnel reflectivity [44] $16\pi^2/Q^4$) for each spin state can be seen in Fig. 6(a). The resulting fit to the spin asymmetry, $SA = [(R^+ - R^-)/(R^+ + R^-)]$, shown in Fig. 6(b) shows a gradient in the magnetization profile, as illustrated in Fig. 6(c) and plotted in Fig. 6(d). While a gradient in the magnetization is observed, the nuclear scattering length density, SLD, exhibits no inhomogeneity [Fig. 6(d)]. This result, sensitive to the atomic density of the film, suggests that the expansion is from He incorporation into the lattice rather than self-interstitials of Sr or Ru. Three alternative models were considered for the spin asymmetry (SA) from PNR; one with a gradient allowing the maximum magnetization to be near the substrate, one with a gradient in the opposite direction, and one with uniform magnetization (shown in SM Fig. 2 [41]). The best fit to the experimental data is an inhomogeneous depth-dependent
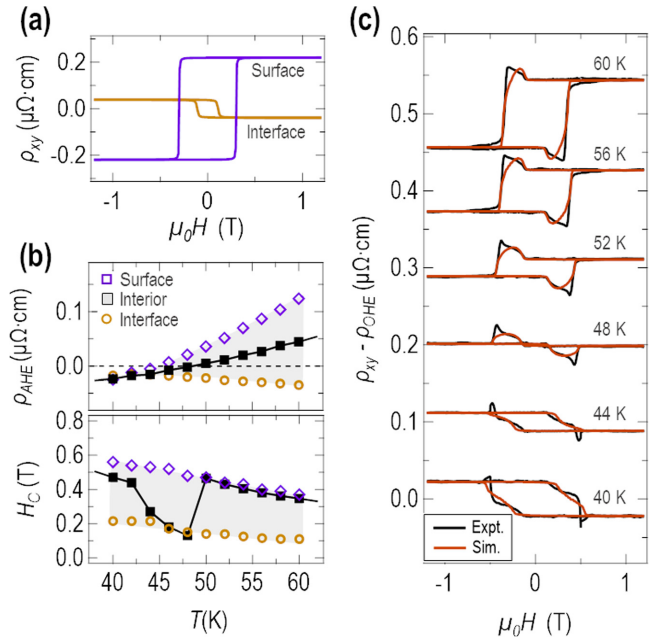
magnetization profile with the lowest magnetization at the surface of the film. Since it is known from magnetometry that an increasing helium dosage results in a decrease in M_S of $SrRuO_3$, the PNR SA is consistent with a helium dose profile in which the largest influence resides near the surface and the lowest influence resides near the film-substrate interface, which is as expected from the SRIM profiles.

To fully describe the role of inhomogeneity on the magnetotransport properties of $SrRuO_3$, we construct a model of the magnetization reversal and AHE using the magnetization profile obtained from PNR as a guide to the depth-dependent variation in intrinsic properties of the $SrRuO_3$. We consider a film consisting of layers with distinct $\rho_{xy,i}(H, T)$, each described by different intrinsic $\rho_{AHE,i}(T)$ and $H_{C,i}(T)$ characteristics. A modified Langevin function is used to describe each component as $\rho_{xy,i}(T, H) = \rho_{AHE,i}(T)[\coth(\beta_i(H \pm H_{C,i}(T)) - 1/\{\beta_i(H \pm H_{C,i}(T))\})]$, where β_i is a term that accounts for the sharpness of the magnetization reversal around H_C that depends on the details of the magnetic domain structure and density [45]. The depth-dependent values for $\rho_{AHE,i}(T)$, $H_{C,i}(T)$, and β_i were taken to vary with depth following the PNR profile shape of Fig. 6(d). The limiting values of the distribution of $\rho_{xy,i}$ and $H_{C,i}$ that represent the surface and interface are shown in Figs. 7(a) and 7(b). The total $\rho_{xy}(T, H)$ of the film is modeled by choosing the limiting values of $\rho_{AHE,i}(T)$ and $H_{C,i}(T)$, and β_i of the surface and film-substrate interface, respectively, as shown in Figs. 7(a) and 7(b), and summed among 1-nm-thick increments of the

film depth accounting for the parallel conduction of the layers [46] (additional details are in SM Fig. 3 [41]).

A comparison of the experimental and modeled $\rho_{xy}(H, T)$ for the SrRuO$_3$ with the largest c_{pc}-axis lattice expansion is shown in Fig. 7(c). The depth-dependent gradient model of the AHE clearly reproduces the characteristic hump-like feature of SrRuO$_3$ in the vicinity of T_R. We note that since the PNR is sensitive only to the film's magnetization, is it possible that a strongly altered surface AHE (e.g., due to inversion symmetry breaking) may account for an additional surface component responsible for the small and sharp kink-like feature observed at the largest applied magnetic fields in Fig. 7(c). However, the multilayer magnetic model provides excellent reproduction of the experimentally observed temperature- and field-dependent AHE while being directly based on the real magnetization profile of the system. This points to the opportunity to predictively design real AHE devices.

These observations also directly address an ongoing topic of debate in the specific SrRuO$_3$ system, where a two-layer or Gaussian inhomogeneity profile has been proposed recently in ultrathin SrRuO$_3$ films, with a proposed origin of the multicomponents attributed to defects or vacancies, substrate-induced octahedral tilting, thickness effects, and inversion symmetry breaking [15,16,23]. The helium irradiation approach produces a depth-dependent inhomogeneity analogous to that observed in ultrathin films, although induced on a macroscopic scale, which can be controlled continuously with helium dosage profile. In addition, the AHE components of the He-irradiated SrRuO$_3$ do not match those of the typical ultrathin SrRuO$_3$, suggesting unique effects of the helium irradiation on the magnetic anisotropy and AHE when a high single-crystal quality is preserved. Finally, it is worth noting that, although a vertical spatial inhomogeneity has been proposed to provide the inversion symmetry breaking necessary for DMI [14], our observation of clear multiple decoupled spin populations present in both $\rho_{AHE}(T)$ and in the $M(H)$ support multiple inhomogeneous ferromagnetic components and not a more complicated explanation of topological Hall effect. Furthermore, our description of the total Hall response from an experimentally derived spatial inhomogeneity profile obtained from neutron reflectometry experiments supports the recent theories that inhomogeneity and resulting multicomponent intrinsic AHE is responsible for the field-dependent hump-like anomalies [15–17,20,21,23] of ultrathin SrRuO$_3$.

In conclusion, combined measurements of x-ray diffraction and polarized neutron reflectometry are used to map the change in crystal structure and magnetization profile through a film thickness. These cross sections are used to provide real space data for a magnetotransport model which shows that magnetic layering alone can generate the anomalous Hall effect observed in SrRuO$_3$ films. We find that the systematic manipulation of lattice symmetry and local distortions possible with helium irradiation is found to be a highly effective means to tune magnetotransport properties driven by Berry phase effects in the prototypical 4d itinerant ferromagnet SrRuO$_3$ and that topological effects do not need to be considered to allow the model to predictively design AHE in this material. These findings enable future studies of Berry phase physics and electronic transport in any epitaxial system with nontrivial states near the Fermi level by providing a post-synthesis method to continuously and iteratively tune structural symmetry and local distortion profiles.

[1] D. Xiao, M.-C. Chang, and Q. Niu, Berry phase effects on electronic properties, Rev. Mod. Phys. **82**, 1959 (2010).

[2] N. Nagaosa, J. Sinova, S. Onoda, A. H. MacDonald, and N. P. Ong, Anomalous Hall effect, Rev. Mod. Phys. **82**, 1539 (2010).

[3] N. P. Armitage, E. J. Mele, and A. Vishwanath, Weyl and Dirac semimetals in three-dimensional solids, Rev. Mod. Phys. **90**, 015001 (2018).

[4] A. Bansil, H. Lin, and T. Das, *Colloquium*: Topological band theory, Rev. Mod. Phys. **88**, 021004 (2016).

[5] A. Neubauer, C. Pfleiderer, B. Binz, A. Rosch, R. Ritz, P. G. Niklowitz, and P. Böni, Topological Hall Effect in the *A* Phase of MnSi, Phys. Rev. Lett. **102**, 186602 (2009).

[6] P. Bruno, V. K. Dugaev, and M. Taillefumier, Topological Hall Effect and Berry Phase in Magnetic Nanostructures, Phys. Rev. Lett. **93**, 096806 (2004).

[7] L. Klein, J. Reiner, T. Geballe, M. Beasley, and A. Kapitulnik, Extraordinary Hall effect in SrRuO$_3$, Physica B **281-282**, 608 (2000).

[8] N. Haham, Y. Shperber, M. Schultz, N. Naftalis, E. Shimshoni, J. W. Reiner, and L. Klein, Scaling of the anomalous hall effect in SrRuO$_3$, Phys. Rev. B **84**, 174439 (2011).

[9] J. Matsuno, N. Ogawa, K. Yasuda, F. Kagawa, W. Koshibae, N. Nagaosa, Y. Tokura, and M. Kawasaki, Interface-driven

topological Hall effect in SrRuO$_3$-SrIrO$_3$ bilayer, Sci. Adv. **2**, e1600304 (2016).

[10] K.-Y. Meng, A. S. Ahmed, M. Baćani, A.-O. Mandru, X. Zhao, N. Bagués, B. D. Esser, J. Flores, D. W. McComb, H. J. Hug, and F. Yang, Observation of nanoscale skyrmions in SrIrO$_3$/SrRuO$_3$ bilayers, Nano Lett. **19**, 3169 (2019).

[11] Y. Gu, Y.-W. Wei, K. Xu, H. Zhang, F. Wang, F. Li, M. S. Saleem, C.-Z. Chang, J. Sun, C. Song, J. Feng, X. Zhong, W. Liu, Z. Zhang, J. Zhu, and F. Pan, Interfacial oxygen-octahedral-tilting-driven electrically tunable topological hall effect in ultrathin SrRuO$_3$ films, J. Phys. D: Appl. Phys. **52**, 404001 (2019).

[12] Y. Ohuchi, J. Matsuno, N. Ogawa, Y. Kozuka, M. Uchida, Y. Tokura, and M. Kawasaki, Electric-field control of anomalous and topological Hall effects in oxide bilayer thin films, Nat. Commun. **9**, 213 (2018).

[13] L. Wang, Q. Feng, Y. Kim, R. Kim, K. H. Lee, S. D. Pollard, Y. J. Shin, H. Zhou, W. Peng, D. Lee, W. Meng, H. Yang, J. H. Han, M. Kim, Q. Lu, and T. W. Noh, Ferroelectrically tunable magnetic skyrmions in ultrathin oxide heterostructures, Nat. Mater. **17**, 1087 (2018).

[14] C. Wang, C.-H. Chang, A. Herklotz, C. Chen, F. Ganss, U. Kentsch, D. Chen, X. Gao, Y.-J. Zeng, O. Hellwig, M. Helm, S. Gemming, Y.-H. Chu, and S. Zhou, Topological Hall effect in single thick SrRuO$_3$ layers induced by defect engineering, Adv. Electron. Mater. **6**, 2000184 (2020).

[15] D. J. Groenendijk, C. Autieri, T. C. van Thiel, W. Brzezicki, J. R. Hortensius, D. Afanasiev, N. Gauquelin, P. Barone, K. H. W. van den Bos, S. van Aert, J. Verbeeck, A. Filippetti, S. Picozzi, M. Cuoco, and A. D. Caviglia, Berry phase engineering at oxide interfaces, Phys. Rev. Research **2**, 023404 (2020).

[16] D. Kan, T. Moriyama, K. Kobayashi, and Y. Shimakawa, Alternative to the topological interpretation of the transverse resistivity anomalies in SrRuO$_3$, Phys. Rev. B **98**, 180408(R) (2018).

[17] L. Wu, F. Wen, Y. Fu, J. H. Wilson, X. Liu, Y. Zhang, D. M. Vasiukov, M. S. Kareev, J. H. Pixley, and J. Chakhalian, Berry phase manipulation in ultrathin SrRuO$_3$ films, Phys. Rev. B **102**, 220406 (2020).

[18] Z. Fang, N. Nagaosa, K. S. Takahashi, A. Asamitsu, R. Mathieu, T. Ogasawara, H. Yamada, M. Kawasaki, Y. Tokura, and K. Terakura, The anomalous Hall effect and magnetic monopoles in momentum space, Science **302**, 92 (2003).

[19] S. Itoh, Y. Endoh, T. Yokoo, S. Ibuka, J.-G. Park, Y. Kaneko, K. S. Takahashi, Y. Tokura, and N. Nagaosa, Weyl fermions and spin dynamics of metallic ferromagnet SrRuO$_3$, Nat. Commun. **7**, 11788 (2016).

[20] L. Wang, Q. Feng, H. G. Lee, E. K. Ko, Q. Lu, and T. W. Noh, Controllable thickness inhomogeneity and Berry curvature engineering of anomalous Hall effect in SrRuO$_3$ ultrathin films, Nano Lett. **20**, 2468 (2020).

[21] B. Sohn, E. Lee, W. Kyung, M. Kim, H. Ryu, J. S. Oh, D. Kim, J. K. Jung, B. Kim, M. Han, T. W. Noh, B.-J. Yang, and C. Kim, Sign-tunable anomalous Hall effect induced by symmetry-protected nodal structures in ferromagnetic perovskite oxide thin films, arXiv:1912.04757.

[22] M. Ziese, L. Jin, and I. Lindfors-Vrejoiu, Unconventional anomalous Hall effect driven by oxygen-octahedra-tailoring of the SrRuO$_3$ structure, J. Phys.: Materials **2**, 034008 (2019).

[23] D. Kan and Y. Shimakawa, Defect-induced anomalous transverse resistivity in an itinerant ferromagnetic oxide, Phys. Status Solidi B **255**, 1800175 (2018).

[24] T. H. Kim, D. Puggioni, Y. Yuan, L. Xie, H. Zhou, N. Campbell, P. J. Ryan, Y. Choi, J.-W. Kim, J. R. Patzner, S. Ryu, J. P. Podkaminer, J. Irwin, Y. Ma, C. J. Fennie, M. S. Rzchowski, X. Q. Pan, V. Gopalan, J. M. Rondinelli, and C. B. Eom, Polar metals by geometric design, Nature **533**, 68 (2016).

[25] A. Herklotz, S. F. Rus, N. Balke, C. Rouleau, E.-J. Guo, A. Huon, S. KC, R. Roth, X. Yang, C. Vaswani, J. Wang, P. P. Orth, M. S. Scheurer, and T. Z. Ward, Designing morphotropic phase composition in BiFeO$_3$, Nano Lett. **19**, 1033 (2019).

[26] A. Herklotz, S. F. Rus, C. Sohn, S. KC, V. R. Cooper, E.-J. Guo, and T. Z. Ward, Optical response of BiFeO$_3$ films subjected to uniaxial strain, Phys. Rev. Mater. **3**, 094410 (2019).

[27] H. Guo, S. Dong, P. D. Rack, J. D. Budai, C. Beekman, Z. Gai, W. Siemons, C. M. Gonzalez, R. Timilsina, A. T. Wong, A. Herklotz, P. C. Snijders, E. Dagotto, and T. Z. Ward, Strain Doping: Reversible Single-Axis Control of a Complex Oxide Lattice via Helium Implantation, Phys. Rev. Lett. **114**, 256801 (2015).

[28] A. Herklotz, A. T. Wong, T. Meyer, M. D. Biegalski, H. N. Lee, and T. Z. Ward, Controlling octahedral rotations in a perovskite via strain doping, Sci. Rep. **6**, 26491 (2016).

[29] J. M. D. Coey, M. Venkatesan, and P. Stamenov, Surface magnetism of strontium titanate, J. Phys.: Condens. Matter **28**, 485001 (2016).

[30] A. Vailionis, H. Boschker, W. Siemons, E. P. Houwman, D. H. A. Blank, G. Rijnders, and G. Koster, Misfit strain accommodation in epitaxial ABO$_3$ perovskites: Lattice rotations and lattice modulations, Phys. Rev. B **83**, 064101 (2011).

[31] W. Lu, P. Yang, W. D. Song, G. M. Chow, and J. S. Chen, Control of oxygen octahedral rotations and physical properties in SrRuO$_3$ films, Phys. Rev. B **88**, 214115 (2013).

[32] L. Klein, J. S. Dodge, C. H. Ahn, G. J. Snyder, T. H. Geballe, M. R. Beasley, and A. Kapitulnik, Anomalous Spin Scattering Effects in the Badly Metallic Itinerant Ferromagnet SrRuO$_3$, Phys. Rev. Lett. **77**, 2774 (1996).

[33] A. Kanbayasi, Magnetic properties of SrRuO$_3$ single crystal, J. Phys. Soc. Jpn. **41**, 1876 (1976).

[34] G. Cao, S. McCall, M. Shepard, J. E. Crow, and R. P. Guertin, Thermal, magnetic, and transport properties of single-crystal Sr$_{1-x}$Ca$_x$RuO$_3$ $<\sim x <\sim$ 1.0, Phys. Rev. B **56**, 321 (1997).

[35] A. Vailionis, W. Siemons, and G. Koster, Room temperature epitaxial stabilization of a tetragonal phase in ARuO$_3$ (A = Ca and Sr) thin films, Appl. Phys. Lett. **93**, 051909 (2008).

[36] A. Herklotz, Z. Gai, Y. Sharma, A. Huon, S. F. Rus, L. Sun, J. Shen, P. D. Rack, and T. Z. Ward, Designing magnetic anisotropy through strain doping, Adv. Sci. **5**, 1800356 (2018).

[37] F. Bern, M. Ziese, K. Dörr, A. Herklotz, and I. Vrejoiu, Hall effect of tetragonal and orthorhombic SrRuO$_3$ films, Phys. Status Solidi R **7**, 204 (2012).

[38] D. Kan, R. Aso, H. Kurata, and Y. Shimakawa, Unit-cell thick BaTiO$_3$ blocks octahedral tilt propagation across oxide heterointerface, J. Appl. Phys. **115**, 184304 (2014).

[39] D. Kan, R. Aso, H. Kurata, and Y. Shimakawa, Epitaxial strain effect in tetragonal SrRuO$_3$ thin films, J. Appl. Phys. **113**, 173912 (2013).

[40] M. Ziese and I. Vrejoiu, Anomalous and planar Hall effect of orthorhombic and tetragonal SrRuO$_3$ layers, Phys. Rev. B **84**, 104413 (2011).

[41] See Supplemental Material at http://link.aps.org/supplemental/ 10.1103/PhysRevB.103.085121 for an illustration of the typical two-component "hump-like" anomaly of ultrathin SrRuO$_3$, and additional details of the depth dependent ferromagnetic inhomogeneity model for polarized neutron reflectometry and Hall effect measurements.

[42] L. G. Parratt, Surface Studies of Solids by Total Reflection of X-Rays, Phys. Rev. **95**, 359 (1954).

[43] P. Kienzle, B. Maranville, K. O'Donovan, J. Ankner, N. Berk, and C. Majkrzak, https://www.nist.gov/ncnr/reflectometry-software, 2017.

[44] S. Singh, M. R. Fitzsimmons, T. Lookman, J. D. Thompson, H. Jeen, A. Biswas, M. A. Roldan, and M. Varela, Magnetic Nonuniformity and Thermal Hysteresis of Magnetism in a Manganite Thin Film, Phys. Rev. Lett. **108**, 077207 (2012).

[45] R. Harrison, A physical model of spin ferromagnetism, IEEE Trans. Magn. **39**, 950 (2003).

[46] R. L. Petritz, Theory of an experiment for measuring the mobility and density of carriers in the space-charge region of a semiconductor surface, Phys. Rev. **110**, 1254 (1958).

[47] U.S. DOE Public Access Plan, http://energy.gov/downloads/ doe-public-access-plan